Earth and Planetary Science Letters 296 (2010) 1–8

Contents lists available at ScienceDirect

Earth and Planetary Science Letters

journal homepage: www.elsevier.com/locate/epsl

Dynamics and structure of a stirred partially molten ultralow-velocity zone

John W. Hernlund *, A. Mark Jellinek

Earth and Ocean Sciences, the University of British Columbia, 6339 Stores Road, Vancouver, Canada BC V6T 1Z4

ARTICLE INFO

Article history:
Received 9 September 2009
Received in revised form 2 April 2010
Accepted 15 April 2010
Available online 1 June 2010

Editor: Y. Ricard

Keywords:
ultralow-velocity zone
partial melt dynamics
core–mantle boundary

ABSTRACT

The seismic properties of thin (5–40 km thickness) patches exhibiting low seismic velocities—termed ultralow-velocity zones or ULVZ—just above the core–mantle boundary (CMB) might be explained by the presence of partially molten rock, where a liquid phase occupies interstices within a skeletal network of solid grains. However, a key problem with this explanation is that in the absence of improbably strong surface tension effects, partial melt is expected to drain by percolation over geological time scales, to form a dense, melt-rich layer at the CMB with physical properties that are inconsistent with seismic and other geophysical constraints. Here we consider whether stirring within ULVZ, driven by viscous coupling to convective motions in the overlying mantle, can inhibit the production of such stratification and maintain a partially molten region with a structure and constitution comparable to what is inferred seismically. We use two-dimensional numerical simulations of the response of a melt–solid mixture to stirring imposed from above and scaling analysis to identify conditions leading to melt separation, retention and drainage over a broad range of parameters. We find that melt migration at plausible ULVZ conditions is governed predominantly by dynamic pressure gradients arising from the viscous deformation related to mantle stirring, rather than by the buoyancy effects driving melt percolation. In particular, dense melt that would otherwise drain downward and accumulate at the CMB is expected to remain in suspension as a result of the stirring driven within ULVZ. In addition, our model predicts that partially molten ULVZ patches will be characterized by a positive gradient in seismic shear velocity (i.e., increasing with depth), consistent with seismic inferences, and may persist in this state over geological time scales.

1. Introduction

Ultralow-velocity zone (ULVZ) material occurs as thin (5–40 km thick) laterally discontinuous patches just above the core–mantle boundary (e.g., Thorne and Garnero, 2004). ULVZ are usually characterized as bodies exhibiting *P* wave velocity (V_P) reductions of ≈10% and *S* wave velocity (V_S) reductions of up to ≈30% (see Lay et al., 2004, for a review). This 3:1 decrement in *S* vs. *P* velocity is potentially diagnostic of a so-called "mush" in which liquid occupies the interstices of a touching solid framework. Viewed this way, the magnitude of the *S*-velocity anomaly can imply melt fractions in the range ≈5–30%, depending on the geometry of the melt-filled pore space (Williams and Garnero, 1996; Berryman, 2000; Hier-Majumder, 2008). In addition, such a decrement imposes important constraints on the structure of these regions. It is, for example, well-known that the connectivity of the solid matrix, which can support elastic stresses in a mush, begins to break down at the percolation threshold, corresponding to melt fractions in the range ≈20–60% (depending on the geometry of the micro-structure). At higher melt concentrations the solid matrix becomes disaggregated into a "slurry" composed of melt and suspended (i.e., unconnected) solid grains that can no longer support elastic stresses (i.e., $V_S = 0$). Partially molten ULVZ patches exhibiting *only* a 3:1 decrement can, thus, only be reliably interpreted as mush. That such mushy regions have not drained (or solidified) over geological time scales presents a remarkable challenge to understanding the current presence and longevity of these regions.

The stabilization of a ULVZ mush against buoyancy-driven melt separation and the resulting production of internal stratification is problematic because the time scale for solid compaction and melt drainage is generally very short in comparison to the age of the Earth (Hernlund and Tackley, 2007). Such issues might be resolved by invoking strong surface tension forces in the micro-mechanical interactions between liquid and solid grains (e.g., Hier-Majumder et al., 2006) or particularly low matrix permeabilities related to very small grain sizes (cf. Eq. (7) and Hernlund and Tackley, 2007). It is, however, difficult to argue that these very special conditions should apply over the full history of the ULVZ regions. Accordingly, in this paper we take a less restrictive approach to the problem and investigate whether the persistence of partial melt over the full depth of ULVZ patches is a natural consequence of drainage that is inhibited by internal stirring driven as a result of viscous coupling to flow in the overlying mantle.

In more detail, to address this problem we use a two-phase dynamics model to investigate the effect of an imposed shear at the

* Corresponding author.
E-mail address: hernlund@gmail.com (J.W. Hernlund).

0012-821X/$ – see front matter © 2010 Elsevier B.V. All rights reserved.
doi:10.1016/j.epsl.2010.04.027

top of a partially molten patch of ULVZ with the geometry shown in Fig. 1. In addition to being consistent with inferences drawn from seismic observations of ULVZ beneath the central Pacific and Africa (e.g., Thorne and Garnero, 2004; others), our picture is supported by laboratory experiments and numerical simulations that show that external convective stresses organize ULVZ-scale dense structures into thicker patches beneath upwelling currents (e.g., Jellinek and Manga, 2002, 2004; Hernlund and Tackley, 2007; McNamara et al., 2008). As a result of the continuity of viscous stresses at the mush–mantle interface such mantle motions will drive vigorous stirring in the relatively low viscosity ULVZ patches (Jellinek and Manga, 2002; Hernlund and Tackley, 2007; McNamara et al., 2008) with a structure that is expected to be comparable to a classical cavity-flow scenario (e.g., Shen and Floryan, 1985). The goal of our work is to build understanding of the effect of this imposed flow on the dynamics of melt retention or drainage in ULVZ mush.

Our most important finding is that under ULVZ-like conditions, buoyancy stresses driving melt percolation are small in comparison to the dynamic pressures induced by the imposed circulation. Thus the distribution of melt inside ULVZ is governed by the migration of melt from regions of high dynamic pressure into regions of low dynamic pressure. This effect causes melt to be driven upward and retained in the matrix even when it is denser than the solid matrix. Our results also lead to a prediction of a ULVZ shear modulus that increases with depth, a feature which would explain the heretofore puzzling inference of an increasing shear velocity with depth inside ULVZ based upon waveform modeling studies (Rost et al., 2006).

2. Model description

We have formulated a numerical two-phase lid-driven cavity-flow model in order to investigate the stability of a mushy ULVZ state when it is stirred by overlying mantle flows (Fig. 2). For simplicity we model a mush in thermodynamic equilibrium at isothermal conditions and for vanishing Reynolds number (i.e., a creeping flow). ULVZ are likely to be approximately isothermal (e.g., Sleep, 1988), being of small thickness (and hence small thermal diffusion time) and overlying an essentially isothermal and inviscid liquid metal outer core (e.g., Braginsky and Roberts, 1995). The model is two-dimensional and unit aspect ratio, and has a length scale denoted as H. All boundaries are taken to be impermeable to both melt and solid flow, while all boundaries except the top support no shear stresses. The lateral velocity of the top is imposed as an external kinematic condition with a maximum value of v_0 and a form that is discussed below. The model equations we use to describe the mechanical evolution of the mush are similar to the mathematical model of two-phase viscous flow developed by Bercovici et al. (2001) and Bercovici and Ricard (2003),

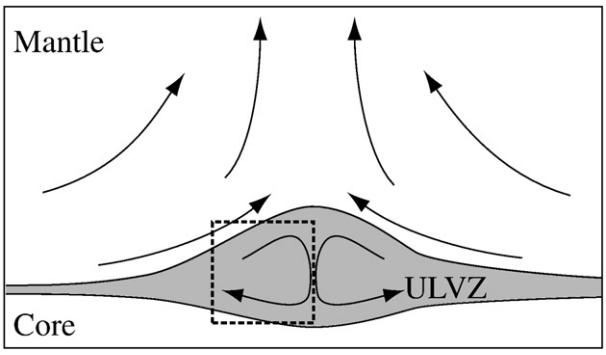

Fig. 1. Schematic illustration of a thickened ULVZ structure entrained beneath an upwelling mantle plume. The velocity of upwelling plume material can be relatively large (of order 1 m/yr or higher; e.g., Jellinek et al., 2003), and the viscosity of the mixture is expected to be relatively small if it is partially molten, thus the ULVZ is stirred by the overlying mantle flows.

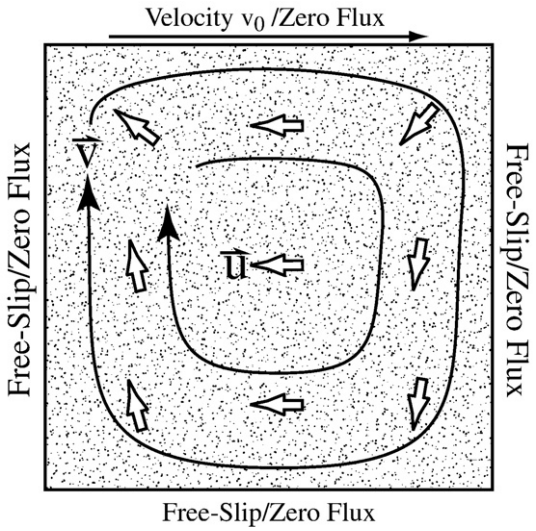

Fig. 2. Cavity-flow configuration used in our numerical models to study the unmixing of a mush in the presence of stirring. All sides are impermeable to flow, and all sides are stress free except the top which has an imposed lateral velocity. The internal mixture velocity $\vec{v}$ assumes the form of a cavity flow, while the Darcy velocity is directed downward owing to a density contrast between the melt and solid which causes downward melt migration.

though with a slight modification (see Appendix A for details) that facilitates numerical solutions with non-homogeneous boundary conditions. In summary, the model includes an equation governing the conservation of the mass of melt,

$$\frac{\partial \phi}{\partial t} + \vec{\nabla}\cdot\left[(1-\phi)\vec{u} + \vec{v}\phi\right] = 0, \tag{1}$$

conservation of total mass, assuming incompressibility of the mixture,

$$\vec{\nabla}\cdot\vec{v} = 0, \tag{2}$$

the force balance in the liquid–solid mixture,

$$\vec{\nabla}\cdot\left(\eta\,\underline{\varepsilon}_v\right) - \vec{\nabla}\tilde{P} + \rho g\hat{z} = 0, \tag{3}$$

and a volume-weighted difference between liquid and solid momenta, or "action–reaction" equation,

$$\frac{\eta_l \vec{u}}{k(\phi)} - \vec{\nabla}\left\{\left[\frac{4}{3}\eta + K_0\eta_s\left(\frac{1-\phi}{\phi}\right)\right]\vec{\nabla}\cdot\vec{u}\right\} = (1-\phi)\Delta\rho g\hat{z} - \left(\vec{\nabla}\tilde{P} + \rho g\hat{z}\right), \tag{4}$$

where,

$$\underline{\varepsilon}_v = \left[\vec{\nabla}\vec{v} + \left(\vec{\nabla}\vec{v}\right)^T\right], \tag{5}$$

and t is time, ϕ is the volume fraction of liquid, $\vec{\nabla}$ is the gradient vector, $\vec{v}$ is velocity (see below), $\vec{u}$ is the Darcy velocity (volume flux per area of liquid through the solid matrix), $\tilde{P} = P + 4/3\vec{\nabla}\cdot\vec{u}$ (P is the isotropic pressure), ρ is the density, g is the upward component of gravitational acceleration, $\hat{z}$ is the upward directed unit vector, η is the mixture viscosity, c_p is the specific heat at constant pressure, $k(\phi)$ is the Darcy permeability, and K_0 is a constant arising from a micro-mechanical model of pore space collapse (Bercovici et al., 2001). A subscript l or s ascribes to the variable, under the two-phase continuum approximation, an average characteristic of the liquid or solid respectively. A quantity preceded by Δ represents the difference between its solid and liquid values, such that $\Delta\rho = \rho_s - \rho_l$. With the

exception of viscosity η which we define below, the lack of a subscript represents that quantity's volume average value over the mixture, e.g., $\vec{v} = \phi\vec{v_l} + (1-\phi)\vec{v_s}$ is the barycentric velocity of the liquid and solid mixture.

We vary the shear viscosity of the mush according to the empirical relation,

$$\eta = \eta_s \exp(-b\phi), \tag{6}$$

where b is a constant. While $b \approx 21$ for basaltic melt in peridotite, this value can vary considerably depending on composition and changes in wetting behavior (e.g., Scott and Kohlstedt, 2006; Hustoft et al., 2007). The permeability k is assumed to depend on ϕ as,

$$k = c_0 \phi^n (1-\phi)^m, \tag{7}$$

where c_0, n, and m are also constants. For melt fractions greater than 40%, the mixture is considered to be a disaggregated slurry (e.g., Saar and Manga, 2002), and we require the viscosity to be small enough so that a surface defined by any contour at $\phi = 40\%$ is essentially shear stress free. For numerical reasons a realistic viscosity reduction across the mush–slurry transition (more than 20 orders of magnitude) cannot be used, however, such a dramatic reduction is not necessary in practice. Numerical experimentation indicates that a value of $10^{-3}\eta_s$ for slurry is already into a limiting regime in which shear stresses between the slurry and mush are largely decoupled, and we therefore use this value for the slurry viscosity. This value is also high enough to suppress the tendency for vigorous (and, in the present context, spurious) convective motions to arise in the slurry in the case where viscosity falls more rapidly, an effect that would otherwise seriously limit the size of time steps in our numerical treatment.

All boundaries except the top are taken to be impermeable and shear stress free. The component of Darcy velocity normal to the boundary vanishes. The average velocity of the mixture at the top assumes the form:

$$\vec{v}_{\text{top}} = v_0 \sin\left(\frac{\pi x}{H}\right)\hat{x}, \tag{8}$$

where $\hat{x}$ is the horizontal unit vector. A sinusoidal form is used to avoid velocity discontinuities and the appearance of strong singularities in stress at the top corners which might otherwise give rise to larger than plausible dynamic pressure gradients. This is important because the dynamics under consideration in this study are intimately related to the magnitude of the dynamic pressure gradient arising from cavity-like circulation driven at the top. Another reason for choosing this particular form is that it allows for simple analytical solutions to be obtained in the case $\phi = $ constant which can be compared to numerical solutions for purposes of validation.

The governing equations can be non-dimensionalized using the length scale H and advective time scale H/v_0, so that the system of equations read,

$$\frac{\partial \phi}{\partial t'} + \vec{\nabla}' \cdot \left[R(1-\phi)\vec{u}' + \vec{v}'\phi\right] = 0, \tag{9}$$

$$\vec{\nabla}' \cdot \vec{v}' = 0, \tag{10}$$

$$\vec{\nabla}' \cdot \left(\eta' \underline{\varepsilon}'_v\right) - \vec{\nabla}' p' + R(\phi - \phi_0)\hat{z} = 0, \tag{11}$$

$$\frac{\vec{u}'}{\delta^2 \phi^n (1-\phi)^m} - \vec{\nabla}'\left\{\left[\frac{4}{3}\eta' + \left(\frac{1-\phi}{\phi}\right)\right]\vec{\nabla}' \cdot \vec{u}'\right\} = (1-\phi)\hat{z} - \frac{\vec{\nabla}' \cdot \left(\eta' \underline{\varepsilon}'_v\right)}{R}, \tag{12}$$

where $t' = tv_0/H$ is the non-dimensional time, $\eta' = \eta/\eta_s$, $\vec{v}' = \vec{v}/v_0$ is the non-dimensional velocity, $\vec{\nabla}' = H\vec{\nabla}$ is the non-dimensional gradient vector, $p' = (\rho_0 g z + P + 4/3\vec{\nabla} \cdot \vec{u})H/\eta_s v_0$, and $\underline{\varepsilon}'_v = \underline{\varepsilon}_v H/v_0$. The non-dimensionalized Darcy velocity is re-written as,

$$\vec{u}' = \frac{\eta_s}{\Delta\rho g H^2}\vec{u} = \frac{1}{R}\frac{\vec{u}}{v_0}. \tag{13}$$

To reduce the degrees of freedom in parameters, we have chosen the constant K_0, which is expected to be of order unity (Bercovici et al., 2001), to be $K_0 = 1$ for all calculations presented here.

Two key non-dimensional parameters appear in the governing equations:

$$\delta^2 = \frac{\eta_s c_0}{\eta_l H^2}, \tag{14}$$

and,

$$R = \frac{\Delta\rho g H^2}{\eta_s v_0}. \tag{15}$$

Physically, R is a ratio of two time scales: a time scale for buoyant diapiric rise of a molten body through a viscous solid matrix $\eta_s/\Delta\rho g H$ to the time scale for the imposed stirring H/v_0. The quantity δ is an effective compaction length that depends critically on the background melt fraction, the melt viscosity and functional form for the permeability and Darcy velocity (see the discussion in Ricard et al., 2001, for further details). In general, δ increases with enhanced permeability and reduced melt viscosity. Thus, for a given melt buoyancy and η_s, a larger δ will lead to a smaller time scale for melt percolation and separation from the matrix.

We solve Eqs. (9)–(12) numerically starting from a uniform melt fraction, $\phi = \phi_0$. We apply the second-order MPDATA method (Smolarkiewicz and Margolin, 1998) to Eq. (9) in order to advance the solution for ϕ forward in time. Solutions for $\vec{u}'$ are obtained using an alternating direction implicit treatment of Eq. (12), and were validated using simple analytical solutions for cases with uniform melt fraction. Solutions for $\vec{v}'$ are found using an iterative staggered grid finite volume approach to Eq. (11) similar to the SIMPLER method of Patankar (1980) and analogous to the kind implemented by Tackley (1996) for solving mantle convection problems with strongly varying viscosity. The accuracy of solutions obtained using the Stokes flow solver are also validated against analytical solutions for simple cases with $\phi = $ constant.

3. Results

Our nominal parameter choices are as follows: $b = (\log 100)/0.4$, yielding two orders of magnitude viscosity decrease up to the disaggregation fraction of 40%, $\phi_0 = 10\%$, $n = 2$, and $m = 0$. R and δ^2 are systematically varied over several orders of magnitude in order to characterize the basic dynamical regimes. In all cases the melt is considered to be more dense than solid, and in the absence of stirring the liquid would accumulate at the lower boundary. We have also experimented with different but reasonable values of b, ϕ_0, and m and find that our main results are insensitive to variations among these parameters.

The basic range of behavior found in the numerical experiments is summarized in Fig. 3, where the melt fraction is shown after integrating forward in time until $t' \approx 25$ (i.e., around 10 overturns or about 10,000 time steps for a grid resolution of 128×128). Results range from cases exhibiting rapid drainage and unmixing of the melt from the solid to form a melt-rich slurry at the bottom corners of the domain overlain by a mostly melt-free solid, cases where melt begins to separate at the boundaries but is readily re-entrained into the circulatory flow, and cases with a well-mixed state where melt fraction variations are essentially negligible.

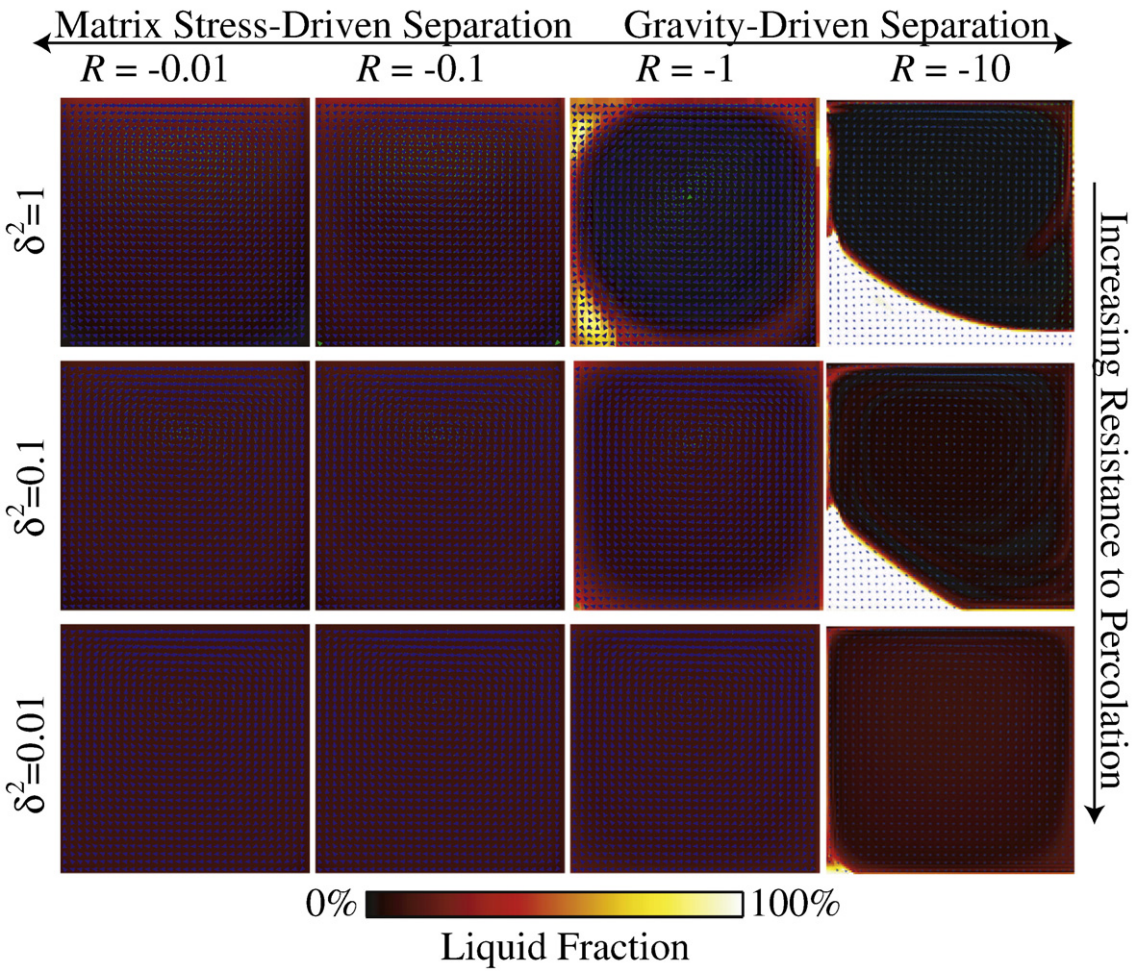

Fig. 3. Melt fraction distributions in the domain after a time integration up to about $t' = 25$ for various values of R and δ^2. The kinds of behaviors in this parameter range capture the essential regimes we have been able to identify in our numerical experiments.

For cases where the magnitude of R exceeds unity (e.g., the $R = -10$ cases in Fig. 3), melt drains to form high melt fraction boundary layers that accumulate at the lower corners, particularly the lower left corner where upwelling flow occurs. Viscous coupling to the solid matrix causes a small fraction of this ponded dense melt to become entrained upward, and after entrainment to the top it is subsequently transported laterally across the domain and then descends back down along the downwelling edge. In most cases, this entrained material moves around the edges of the domain without significantly affecting melt fraction in the core of the circulation, which grows increasingly melt depleted over time.

By contrast, as the magnitude of R approaches unity, the volume of dense melt carried upward and maintained near the top of the domain increases. At $R = 1$ there are approximately equal volumes of melt ponded at the top and bottom corners. For $R < 1$ the tendency for melt to be retained within the matrix, above the bottom boundary, is enhanced. Moreover, this accumulation of melt at the top of the domain tends towards a steady state in which the rate of upward melt migration is balanced by the rate of downward melt percolation.

For the entire range of R values, the magnitude of melt fraction variations after several over turns is modulated by δ^2, which governs the rate of compaction. In our model, δ^2 appears to play the relatively simple role of modulating the rate of percolation and separation of melt and solid to form melt-enriched regions. In the $R < 1$ cases that approach steady state over time, for example, δ^2 modulates only the time scale required to reach steady conditions and does not influence the basic structure of the resulting mixture. Therefore, R appears to be the most important factor governing the steady state structure of a stirred mush.

4. Interpretation

We observe that as $R \to 0$, effects arising from stirring become more important than flow driven by buoyancy effects. Melt separation occurs in these cases but is related to the tendency of gradients in stress to drive melt migration rather than gravity acting on a melt of different density than the solid. This kind of behavior is similar to that described by Spiegelman and McKenzie (1987), where it was shown that the scale length over which melt was re-directed toward the corner of a viscous cavity flow is given by a "piezometric length scale" $L = \sqrt{\eta_s v_0 / (1-\phi_0)\Delta\rho g}$, which is obtained by equating the time scales for stirring and melt drainage. In terms of the present non-dimensionalization, this length is $L' = 1/\sqrt{R(1-\phi_0)}$. Thus for $R < 1$, we find that $L' > 1$, implying that melt percolation over the domain depth H is inhibited because the length scale for melt migration driven by matrix shear stresses is in excess of the domain itself. Said differently, this result indicates that the time scale for percolation is sufficiently long in comparison to the time scale for imposed stirring that buoyancy-driven melt drainage becomes an unimportant process.

The piezometric length scale identifies only a basic condition for melt retention. Dynamically, the modulation of melt migration by variations in R can be better understood in terms of a competition of

the driving pressure gradients. Darcy's law (e.g., Eq. (4)) written in any form invariably contains the following proportionality,

$$\vec{u} \propto -\vec{\nabla} p - \Delta\rho \vec{g}. \tag{16}$$

Thus, the flow of liquid through pore space is driven down the dynamic pressure gradient $-\vec{\nabla} p$, which acts towards the corners of the domain (Fig. 4), and by pressure gradients related to lateral differences in hydrostatic pressure (i.e., buoyancy effects) $-\Delta\rho\vec{g}$ that act in the direction of gravity (i.e., downward). The dynamic pressure gradient therefore drives melt upward, replenishing the top of the domain in liquid, while gravity tends to make dense liquids sink and accumulate at the bottom. The ratio of these two pressure gradients is,

$$\frac{\Delta\rho g}{\vec{\nabla} p} \approx \frac{\Delta\rho g H^2}{\eta_s v_0} = R, \tag{17}$$

and therefore upward directed forcing becomes dominant when $R<1$ while downward directed forcing is dominant when $R>1$. It is interesting to note that we arrive at this result as a simple ratio of forces on the right-hand side of the Darcy equation alone, independently of the details and treatment of viscous compaction.

The existence of a state for $R<1$ in which dense melt has accumulated near the top of the mushy region but then stops accumulating further implies a dynamic balance. Stirring gives rise to a kinematic flow that transports accumulated melt laterally across the top of the domain and then downward on the descending side. However, instead of descending, the melt enrichment remains at the top in these cases owing to upward migration at a rate that balances the rate of downward transport in the stirred flow. A possible cause of this behavior is the viscosity reduction near the top of the domain owing to accumulation of melt, which partly lubricates the flow driven at the boundary. Such lubrication can reduce the dynamic pressure gradient that causes melt to migrate upward until it balances the tendency to be mixed downward. This would be a stable equilibrium because any depletion of melt near the top would increase the viscosity and the dynamic pressure gradient and subsequently the upper region would be replenished by enhanced upward melt migration. On the other hand, any slight enrichment in melt would decrease the pressure gradient and allow excess melt to be transported downward by the kinematic flow.

5. Implications for ULVZ

To apply our results it is important to first consider the physical properties, structure and constitution of ULVZ in greater detail. As a whole, ULVZ patches exhibit a density increase relative to surrounding mantle, and exist as gravitationally stable layers with a density intermediate between the deep mantle and core. This basic picture is supported by analyses of short period ($\approx$1 s) seismic waves. For example, Rost et al. (2006) used short period waveform modeling of interaction of the *ScP* phase with a ULVZ-rich region beneath the southwest Pacific to show that ULVZ material is about 8% denser than average mantle. Rost et al. demonstrate that a less dense ULVZ is implausible because it would require a polarity for *ScP* precursors that is opposite to that which is observed in data covering the southwest Pacific. Numerical models of convection and melting at the base of the mantle also demonstrate that such features can only be compatible with ULVZ if the molten region is dense (Hernlund and Tackley, 2007).

Because of the high pressure at the CMB atomic configurations in the solid and liquid phases are similar and close to optimal packing. A phase change will consequently be characterized by a molar volume difference of only around 1% (Williams and Garnero, 1996). Densification of the melt by relative enrichment in iron or other heavy atomic species in favor of lighter species may also enhance the density difference between liquid and solid, but this depends on the phase diagram which is not well-constrained at the present time. Nevertheless, the large density contrasts implied by Rost et al. (2006) cannot be reasonably explained by a change in phase alone, and demand that ULVZ have an intrinsically different bulk composition such as an increase in overall FeO abundance relative to MgO. Such a compositional difference and the existence of a mush could very well be correlated: an Fe-enriched composition not only increases the ULVZ density but simultaneously depresses the solidus temperature to enable the thermodynamic stability of a liquid phase. This picture is reasonable and a plausible outcome following fractional crystallization of an ancient long-lived basal magma ocean (Labrosse et al., 2007), in which case ULVZ is interpreted to be the mushy residue of a previously much larger magma body.

From the results of Rost et al., the 1% liquid–solid density difference expected from the experiments of Williams and Garnero (1996) and geodynamic constraints on mantle convective velocities in the deep mantle we can place bounds on the value of R appropriate for ULVZ. Accordingly, we take the density difference between the ULVZ and surrounding mantle $\Delta\rho_{\mathrm{ULVZ}}$ to be in the order of 10% and the density difference between the solid and liquid phases $\Delta\rho$ to be in the order of 1%. Assuming that the ULVZ topography is supported by viscous forces arising from flows in the overlying mantle, continuity of viscous stresses at the mantle–ULVZ interface yields a constraint upon the ULVZ circulation velocity v_0 (e.g., Jellinek and Manga, 2002),

$$v_0 \approx \frac{\Delta\rho_{\mathrm{ULVZ}} g H^2}{\eta}, \tag{18}$$

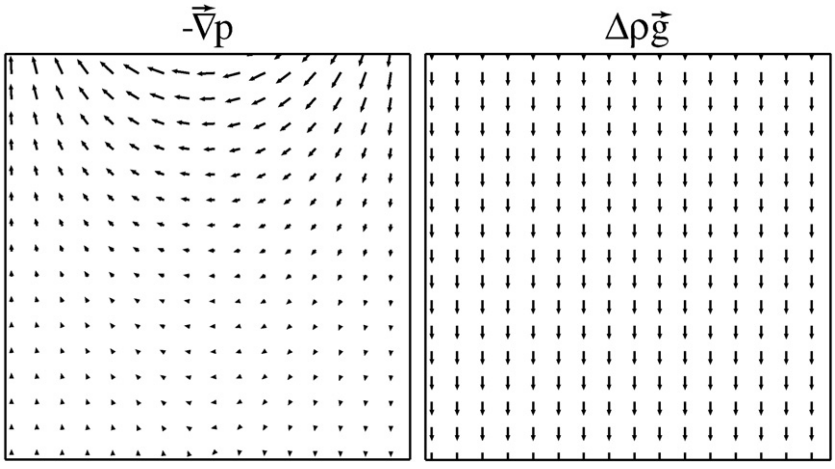

Fig. 4. Illustration of the opposing directions of melt migration force arising from dynamic pressure gradients due to stirring vs. the downward force of gravity acting on a dense melt.

which leads, in turn, to

$$R \approx \frac{\Delta\rho}{\Delta\rho_{ULVZ}} \frac{\eta}{\eta_s}. \quad (19)$$

Using values stated above, and noting that $\eta < \eta_s$ (i.e., a partial molten mixture has smaller viscosity than the solids in the mixture), we find that R should be smaller than unity, and perhaps by more than one order of magnitude (i.e., $R < 0.1$). From the results (e.g., Fig. 3) this estimate implies that ULVZ should be well into the stirring-dominated regime in which buoyancy (i.e., gravity) plays little or no role in the dynamics of melt separation. Indeed, the estimates used above to obtain this value would have to be in error by more than one order of magnitude to change this conclusion, which in this case seems unlikely. Note also that this estimate for R depends only on density and viscosity ratios, neither of which could plausibly be greater than unity.

ULVZ in such a stirring-dominated regime should be melt-enriched near the top relative to the bottom. This picture predicts, in turn, that seismic velocities, which generally decrease with increasing melt fraction, can exhibit an *increase* with depth inside the ULVZ. Such a velocity increase gradient inside ULVZ has been reported by Rost et al. (2006) by modeling high frequency *ScP* data. Indeed, to obtain a reasonable fit to *ScP* coda it was found necessary to include a positive gradient in velocity, even though there was no obvious reason to expect such a feature. While modeling of coda is less secure than modeling of pre-cursory energy due to possible contamination from out-of-plane scattering, this correspondence between our predictions and the seismic modeling is notable.

It is also interesting to consider the present results in the broader context of the evolution of Earth's deep mantle and core. Cooling of Earth's deep interior over geologic time is necessary to drive convection inside the core that has sustained a geodynamo for at least the past 3.2 billion yr (Tarduno et al., 2007), and implies that any partially molten ULVZ must be the remnants of a much thicker "basal magma ocean" (BMO) that would have formed early in Earth's history (Labrosse et al., 2007). In this scenario, buffering of heat capacity by the underlying core and slow cooling by solid state convection in the overlying mantle would have led to a gradual crystallization that led naturally to a state in which ULVZ are iron-enriched, dense, and buffered at the liquidus–solidus by fractionation (Labrosse et al., 2007). A stable BMO requires a slightly higher melt density relative to mantle solids in equilibrium and a relatively large Gruneisen parameter in the liquid state, and these effects are expected at deep mantle conditions based upon extrapolations using equations of state determined by static experiments at lower pressures (e.g., Ohtani and Maeda, 2001), ab initio models of silicate liquids (e.g., Stixrude and Karki, 2005), and shock wave experiments (Akins et al., 2004; Mosenfelder et al., 2007). Clearly, further resolution of the state of ULVZ will shed much light on this process and the manner in which deep mantle melts have evolved with time. Given the important consequences for geochemistry and Earth's early thermal evolution (Labrosse et al., 2007), these issues surrounding ULVZ remain at the frontier of our understanding of deep Earth processes and should motivate further seismological and theoretical studies.

The present results suggest a length scale that selects for ULVZ as a mushy object that is modulated by the appropriate physical and dynamical parameters in the deep mantle. For example, in Earth's past when conditions were hotter, a thicker region of melt such as a BMO would not have been stable as a mush because the magnitude of R was of order unity or greater. This is because $R = \delta\rho g H^2/\eta_s v_0$, and there is a strong dependence on thickness H such that R would be expected to have been significantly larger in the past. I.e., while η_s and/or v_0 might have been slightly different, neither can reasonably be expected to have changed more than order H^2 according to the results of basic thermal evolution models (Labrosse et al., 2007), and therefore the transition from a slurry-like mostly liquid BMO to a state allowing for the formation of a mushy ULVZ might have occurred when the molten region grew smaller than a critical size $H_{crit} \approx \sqrt{\eta_s v_0 / \delta\rho g}$ (i.e., similar to the "piezometric" length scale L' discussed in the previous section). A slurry–mush transition in time from $H > H_{crit}$ to $H < H_{crit}$ would also have consequences for the chemical evolution of the very bottom of Earth's mantle, such as accommodating a change from fractional to batch crystallization which would in turn affect the evolution in composition of both liquid and solid phases.

While not the focus of the present study, the movement of melt through other portions of Earth's mantle is also important and it is interesting to consider where this other category of problems exists in the context of the present model and parameters. One example where similar kinds of issues play an essential role is the retention of small amounts of partial melt in Earth's asthenosphere, which might be capable of producing large seismic velocity contrasts with the overlying lithosphere (Rychert and Shearer, 2009; Kawakatsu et al., 2009). In this case, the asthenosphere is also being deformed by the motion of lithospheric plates, although its response may not be as simple as a cavity-like flow. However, in direct analogy with the ULVZ problem, if melt was not able to be retained as a dynamically stable mush then partial melt would not remain a viable mechanism for explaining this particular kind of seismic velocity change. Although other dynamics such as those relating to buoyant melting are also important and need to be considered at the scales relevant to the upper mantle (e.g., Stevenson, 1988; Tackley and Stevenson, 1993; Raddick et al., 2002; Hernlund et al., 2008a,b), it is still instructive to examine the rate of percolation modulated by δ^2 and competition between melt buoyancy and stirring measured by R. An estimate of δ^2 (using $\eta_s/\eta_l = 10^{19}$, $H = 100$ km, and $c_0 = d^2/72\pi$ with grain size $d = 1$ cm) yields values of order 100. An estimate of R (using $\Delta\rho = 500$ kg/m^3, $g = 10$ m/s^2, $H = 100$ km, $\eta_s = 10^{19}$ Pa s, and $v_0 = 1$ cm/yr) yields values of order 10,000. Therefore, the asthenospheric scale problem is one where melt buoyancy is dominant and percolation of melt out of the asthenosphere is expected to be very rapid. Thus unlike ULVZ, the effects of stirring can be largely ignored at asthenospheric scales. The impact of matrix forcing effects on drainage of melt over different length scales in the upper mantle was also examined by Ribe (1985), who similarly concluded that at scales much larger than several km melt buoyancy becomes the dominant force. The propensity for coherent melt drainage by percolation at large scales may present a dilemma for the retention of melt throughout the asthenosphere, unless effects such as hydrous melting can alter this behavior in a manner that substantially reduces the magnitude of R.

6. Conclusions

In summary, the dynamics of a partially molten system in the presence of gravity and stirring are governed by two non-dimensional parameters, $\delta^2 = (\eta_s/\eta_l)(c_0/H^2)$ which modulates the rate of relative motion between melt and solid, and $R = \delta\rho g H^2/\eta_s v_0$ which measures the importance of melt buoyancy relative to stirring-induced dynamic pressure gradients. The results of the two-phase dynamics models demonstrate that the behavior trend for $|R| > 1$ is always toward a slurry-dominated mixture in the lower upwelling corner overlain by a melt-free solid and a slight degree of mush due only to entrainment of a small mushy boundary layer upward and around the edges of the domain. For $|R| \leq 1$ forces arising from stirring become dominant, melt buoyancy is insignificant, and melt migrates upward even when the melt is denser than the solids. For reasonable force balances supporting ULVZ topography in the deep mantle, we argue that $|R| < 1$ and therefore ULVZ are likely to be in the stirring dominant regime. This predicts that ULVZ may be enriched in melt at the top, and relatively depleted in liquid at the bottom, in accordance with seismic inferences.

The results of this study contradict several conclusions of Hernlund and Tackley (2007), and allow for a viable mechanism to retain melt inside ULVZ in a way that is sufficient to explain their anomalously low shear modulus. The reason the previous study did not arrive at this possibility is that the migration of melt was considered only in the simple context of melt percolation driven by gravity alone. In the present study, it was found that gravity is largely irrelevant and that matrix stresses (which were not previously included in the force balances) are dominant in this context. Furthermore, the smaller viscosity of a partially molten ULVZ subjects these bodies to stirring motions driven by viscous stresses originating from thermal convection in the overlying mantle. While such viscosity variations were considered to be unimportant previously, those models were much larger in scale (i.e., 500 km thickness) and it is doubtful that any kinematic effects arising from stirring would have been adequately resolved.

Acknowledgements

We thank Josef Dufek, Saswata Hier-Majumder, Thorne Lay, and Dave Stegman for discussions that helped to shape the direction and clarified the results of this study. We are grateful for reviews by Allen McNamara and Ondřej Šrámek which considerably improved the manuscript. This work was supported by the Canadian Institute for Advanced Research, Earth Systems Evolution Program, and a grant from the National Science Foundation (NSF EAR 0855737).

Appendix A. Model equations and assumptions

Many mathematical models for treating two-phase dynamics have been proposed (e.g., McKenzie, 1984; Ribe, 1985; Scott and Stevenson, 1986; Spiegelman, 1993; Schmeling, 2000; Bercovici et al., 2001; Bercovici and Ricard, 2003). The recent model proposed by Bercovici and Ricard (2003) has been shown to be formally equivalent to the governing equations of McKenzie (1984) in limiting circumstances, which helps to moderate concerns regarding differences in various formulations. Here we adopt the so-called "geologically relevant limit" of a solid viscosity which is much larger than the liquid viscosity ($\eta_s >> \eta_l$) and a surface energy which is primarily partitioned into the solid phase(s). We additionally neglect surface tension. In the nomenclature of Bercovici and Ricard (2003) this amounts to setting $\sigma = f^* = \omega = 0$. We then obtain a momentum equation for the mixture (Bercovici and Ricard, 2003, see Eqs. (31)–(35)),

$$\vec{\nabla}\cdot\underline{\tau} - \vec{\nabla}P - \rho g\hat{z} = 0, \tag{A1}$$

and a volume-weighted difference between liquid and solid momenta, or "action–reaction" equation,

$$\frac{\eta_l \vec{u}}{k(\phi)} - \vec{\nabla}\left[K_0\eta_s\left(\frac{1-\phi}{\phi}\right)\vec{\nabla}\cdot\vec{u}\right] = (1-\phi)\Delta\rho g\hat{z} - \vec{\nabla}\cdot\underline{\tau} = (1-\phi)\Delta\rho g\hat{z} - \left(\vec{\nabla}P + \rho g\hat{z}\right), \tag{A2}$$

where $\underline{\tau}$ is the deviatoric stress of the mixture. Eq. (A1) describes the average force balance in the melt–solid mixture, while Eq. (A2) governs the forces that drive separation of melt and solid. Below we describe modifications to Eqs. (A1) and (A2) that we employ in order to treat mixture viscosity more realistically, to simplify the boundary conditions for cavity flow, and to eliminate a coupling between melt migration and matrix shear stress that allows for a simple sequential solution procedure.

Bercovici et al. (2001) proposed that the simplest possible choice for the mixture stress assumes the form,

$$\underline{\tau} = \phi\,\underline{\tau}_l + (1-\phi)\,\underline{\tau}_s, \tag{A3}$$

where,

$$\underline{\tau}_s = \eta_s\left[\vec{\nabla}\vec{v}_s + \left(\vec{\nabla}\vec{v}_s\right)^T - \frac{2}{3}\vec{\nabla}\cdot\vec{v}_s\,\underline{I}\right], \tag{A4}$$

and,

$$\underline{\tau}_l = \eta_l\left[\vec{\nabla}\vec{v}_l + \left(\vec{\nabla}\vec{v}_l\right)^T - \frac{2}{3}\vec{\nabla}\cdot\vec{v}_l\,\underline{I}\right] \tag{A5}$$

and $\underline{I}$ is the identity tensor. Note that η_s and η_l in this derivation are taken to be the viscosities relevant to each of the individual phases, and therefore do not depend on any other properties of the mixture. Therefore, in the limit $\eta_s \gg \eta_l$ the mixture stress becomes,

$$\underline{\tau} \to (1-\phi)\underline{\tau}_s = (1-\phi)\eta_s\left[\vec{\nabla}\vec{v}_s + \left(\vec{\nabla}\vec{v}_s\right)^T - \frac{2}{3}\vec{\nabla}\cdot\vec{v}_s\,\underline{I}\right], \tag{A6}$$

and the effective viscosity of the mixture obtained using solid velocity as the proxy for strain-rate (i.e., the case applicable to mushes) would vary like,

$$\eta = (1-\phi)\eta_s, \tag{A7}$$

Because η_s is independent of ϕ in this theory, the viscosity of the mixture is imposed to vary linearly between $\eta_l = 0$ (for a completely liquid state) and η_s (for a melt-free solid) as melt fraction is varied.

This simple linear variation in η with ϕ presents a problem because experimental evidence points to a more sensitive and complex pattern of mixture viscosity variations. In particular, the behavior observed for ϕ less than the disaggregation fraction (i.e., mush) is usually fit to the empirical relation,

$$\eta = \eta_s \exp(-b\phi), \tag{A8}$$

where b is a constant. This kind of behavior is observed regardless of whether the liquid is silicate (e.g., Scott and Kohlstedt, 2006) or metallic (e.g., Hustoft et al., 2007), and these kinds of experiments indicate that η may decrease by 2–3 orders of magnitude as ϕ increases from zero up to the disaggregation fraction. Furthermore, the decrease in mixture viscosity above the disaggregation fraction is precipitous, almost immediately assuming the value of liquid viscosity in the slurry state. The differences between the simple linear variation predicted by the Bercovici and Ricard (2003) model for mixture stress and empirical observations are therefore significant and should be reconciled. As a simple fix for our present purposes, we will instead adopt a mixture viscosity that varies exponentially, as in Eq. (A8), and for ϕ above the disaggregation fraction we impose the smallest value of viscosity that can be tolerated by our numerical solver in order to mimic the essential behavior of slurry. However, note that we treat η_s and η_l as fixed parameters where they appear in all other terms in the governing equations.

Another issue introduced by the two-phase cavity-flow problem is that of imposing velocity at one of the boundaries. We have found that it is convenient to fix the mixture velocity at the boundary, which is defined as $\vec{v} = \phi\vec{v}_l + (1-\phi)\vec{v}_s$ (i.e., the volume average velocity of the mixture). Using this velocity, flow is driven at the top in the same manner independently of the state of material (i.e., mush vs. slurry) adjacent to the boundary. We then make a further approximation that considerably simplifies the solution procedure, by exploiting the presumably weak coupling between melt migration and mixture shear stress. In particular, noting that $\vec{v}_s = \vec{v} - \vec{u}$, we make the following approximation:

$$\vec{\nabla}\cdot\underline{\tau} = \vec{\nabla}\cdot\left[(1-\phi)\underline{\tau}_s\right] = \vec{\nabla}\cdot\left[\eta\left(\underline{\varepsilon}_v - \underline{\varepsilon}_u\right)\right] \approx \vec{\nabla}\cdot\left(\eta\,\underline{\varepsilon}_v\right) - \vec{\nabla}\left(\frac{4}{3}\eta\vec{\nabla}\cdot\vec{u}\right) \tag{A9}$$

where,

$$\underline{\varepsilon_v} = \vec{\nabla}\vec{v} + \left(\vec{\nabla}\vec{v}\right)^T, \tag{A10}$$

and,

$$\underline{\varepsilon_u} = \vec{\nabla}\vec{u} + \left(\vec{\nabla}\vec{u}\right)^T - \frac{2}{3}\vec{\nabla}\cdot\vec{u}\,\underline{I}. \tag{A11}$$

Note that there is no divergence term for $\underline{\varepsilon_v}$ because $\vec{\nabla}\cdot v = 0$. The term proportional to divergence of Darcy velocity in Eq. (A9) is retained in order to account for divergence of stress that accompanies compaction of the solid matrix, and the choice of 4/3 as a coefficient is motivated by the fact that in uni-axial compression along an axis z the term $\vec{\nabla}\cdot\underline{\varepsilon_u}$ becomes $\frac{4}{3}\partial^2 u/\partial z^2$, or $\frac{4}{3}\partial/\partial r\left(\vec{\nabla}\cdot\vec{u}\right)$ in radial compression. The mixture momentum Eq. (A1) is then,

$$\vec{\nabla}\cdot\left(\eta\underline{\varepsilon_v}\right) - \vec{\nabla}\tilde{P} + \rho g\hat{z} = 0, \tag{A12}$$

where $\tilde{P} = P + 4/3\eta\vec{\nabla}\cdot\vec{u}$. For the action–reaction Eq. (A2) we then have,

$$\frac{\eta_l\vec{u}}{k(\phi)} - \vec{\nabla}\left\{\left[\frac{4}{3}\eta + K_0\eta_s\left(\frac{1-\phi}{\phi}\right)\right]\vec{\nabla}\cdot\vec{u}\right\} = (1-\phi)\Delta\rho g\hat{z} - \left(\vec{\nabla}\tilde{P} + \rho g\hat{z}\right). \tag{A13}$$

An important practical advantage gained by the approximation (Eq. (A9)) is that one may solve Eq. (A12) for v and P (using $\vec{\nabla}\cdot v = 0$ as a constraint) independently of Eq. (A13) or any prior knowledge of $\vec{u}$. After a solution for $\tilde{P}$ is obtained, then Eq. (A13) may be solved with terms involving $\tilde{P}$ entering as a right-hand side forcing term. Thus any existing Stokes solver may be used for Eq. (A12), and further code for solving Eq. (A12) can be added as a purely sequential process to obtain solutions for $\vec{u}$. Thus our present approximation eliminates a coupling between matrix shear stress and melt migration that would otherwise require simultaneous solutions of the mixture momentum and action–reaction equations. We believe this one-way dynamic coupling from the solid to the liquid phase is a reasonable approximation in the present scenario, and a posteriori comparisons of the importance of the neglected terms verify that they are always small in comparison to the contribution of solid shear to mixture stress.

References

Akins, J.A., Luo, S.-N., Asimow, P.D., Ahrens, T.J., 2004. Shock-induced melting of $MgSiO_3$ and implications for melts in Earth's lowermost mantle. Geophys. Res. Lett. 31, L14612.

Bercovici, D., Ricard, Y., 2003. Energetics of a two-phase model of lithospheric damage, shear localization and plate boundary formation. Geophys. J. Int. 152, 581–596.

Bercovici, D., Ricard, Y., Schubert, G., 2001. A two-phase model for compaction and damage 1. General theory. J. Geophys. Res. B 106, 8887–8906.

Berryman, J.G., 2000. Seismic velocity decrement ratios for regions of partial melt in the lower mantle. Geophys. Res. Lett. 27, 421–424.

Braginsky, S.I., Roberts, P.H., 1995. Equations governing convection in Earth's core and the geodynamo. Geophys. Astrophys. Fluid Dyn. 79, 1–97.

Hernlund, J.W., Tackley, P.J., 2007. Some dynamical consequences of partial melting at the base of Earth's mantle. Phys. Earth Planet. Inter. 162, 149–163.

Hernlund, J.W., Stevenson, D.J., Tackley, P.J., 2008. Buoyant melting instabilities beneath extending lithosphere. 2. Linear analysis. J. Geophys. Res. 113, B04406.

Hernlund, J.W., Tackley, P.J., Stevenson, D.J., 2008. Buoyant melting instabilities beneath extending lithosphere. 1. Numerical models. J. Geophys. Res. 113, B04405.

Hier-Majumder, S., 2008. Influence of contiguity on seismic velocities of partially molten aggregates. J. Geophys. Res. 113, B12205. doi:10.1029/2008JB005662.

Hier-Majumder, S., Ricard, Y., Bercovici, D., 2006. Role of grain boundaries in magma migration and storage. Earth Planet. Sci. Lett. 248, 735–749.

Hustoft, J., Scott, T., Kohlstedt, D.L., 2007. Effect of metallic melt on the viscosity of peridotite. Earth Planet. Sci. Lett. 260, 355–360.

Jellinek, A.M., Manga, M., 2002. The influence of a chemical boundary layer on the fixity, spacing, and lifetime of mantle plumes. Nature 418, 760–763.

Jellinek, A.M., Manga, M., 2004. Links between long-lived hot spots, mantle plumes, D″, and plate tectonics. Rev. Geophys. 42, 3002.

Jellinek, A.M., Gonnermann, H.M., Richards, M.A., 2003. Plume capture by divergent plate motions: implications for the distribution of hotspots, geochemistry of mid-ocean ridge basalts, and estimates of the heat flux at the core–mantle boundary. Earth Planet. Sci. Lett. 205, 361–378.

Kawakatsu, H., Kumar, P., Takei, Y., Shinohara, M., Kanazawa, T., Araki, E., Suyehiro, K., 2009. Seismic evidence for sharp lithosphere–asthenosphere boundaries of oceanic plates. Science 324, 499–502. doi:10.1126/science.1169499.

Labrosse, S., Hernlund, J.W., Coltice, N., 2007. A crystallizing dense magma ocean at the base of the Earth's mantle. Nature 450, 866–869.

Lay, T., Garnero, E.J., Williams, Q., 2004. Partial melting in a thermo-chemical boundary layer at the base of the mantle. Phys. Earth Planet. Int. 146, 441–467.

McKenzie, D., 1984. The generation and compaction of partially molten rock. J. Petrol. 25, 713–765.

McNamara, A.K., Garnero, E.J., Rost, S., Thorne, M.S., 2008. Dynamics of the ultra low velocity zone. Eos Trans. AGU 89 (53), Fall Meet. Suppl., Abstract DI24A-04.

Mosenfelder, J.L., Asimow, P.D., Ahrens, T.J., 2007. Thermodynamic properties of Mg_2SiO_4 liquid at ultra-high pressures for shock measurements to 200 GPa on forsterite and wadsleyite. J. Geophys. Res. 112, B06208.

Ohtani, E., Maeda, M., 2001. Density of basaltic melt at high pressure and stability of the melt at the base of the lower mantle. Earth Planet. Sci. Lett. 193, 69–75.

Patankar, S.V., 1980. Numerical Heat Transfer and Fluid Flow. Hemisphere Publishing Corp, Washington, DC. 210 pp.

Raddick, M.J., Parmentier, E.M., Scheirer, D.S., 2002. Buoyant decompression melting: a possible mechanism for intraplate volcanism. J. Geophys. Res. B 107.

Ribe, N.M., 1985. The deformation and compaction of partial molten zones. Geophys. J. Int. 83, 487–501.

Ricard, Y., Bercovici, D., Schubert, G., 2001. A two-phase model for compaction and damage. 2. Applications to compaction, deformation, and the role of interfacial surface tension. J. Geophys. Res. B 106, 8907–8924.

Rost, S., Garnero, E.J., Williams, Q., 2006. Fine-scale ultralow-velocity zone structure from high-frequency seismic array data. J. Geophys. Res. 111, B09310.

Rychert, C.A., Shearer, P.M., 2009. A global view of the lithosphere–asthenosphere boundary. Science 324, 495–498. doi:10.1126/science.1169754.

Saar, M.O., Manga, M., 2002. Continuum percolation for randomly oriented soft-core prisms. Phys. Rev. E 650 (5), 056131. doi:10.1103/PhysRevE.65.056131.

Schmeling, H., 2000. Partial melting and melt segregation in a convecting mantle. In: Bagdassarov, N., Laporte, D., Thompson, A.B. (Eds.), Physics and Chemistry of Partially Molten Rocks. Kluwer Academic Publ., pp. 141–178.

Scott, T., Kohlstedt, D.L., 2006. The effect of large melt fraction on the deformation behavior of peridotite. Earth Planet. Sci. Lett. 246, 177–187.

Scott, D.R., Stevenson, D.J., 1986. Magma ascent by porous flow. J. Geophys. Res. 91, 9283–9296.

Shen, C., Floryan, J.M., 1985. Low Reynolds number flow over cavities. Phys. Fluids 28, 3191–3202.

Sleep, N.H., 1988. Gradual entrainment of a chemical layer at the base of the mantle by overlying convection. Geophys. J. 95, 437–447.

Smolarkiewicz, P.K., Margolin, L.G., 1998. MPDATA: a finite-difference solver for Geophysical flows. J. Comp. Phys. 140, 459–480.

Spiegelman, M., 1993. Flow in deformable porous media, part 1, simple analysis. J. Fluid Mech. 247, 17–38.

Spiegelman, M., McKenzie, D., 1987. Simple 2-D models for melt extraction at mid-ocean ridges and island arcs. Earth Planet. Sci. Lett. 83, 137–152.

Stevenson, D.J., 1988. Rayleigh–Taylor instabilities in partially molten rock. EOS 69, 1404.

Stixrude, L., Karki, B., 2005. Structure and freezing of $MgSiO_3$ liquid in Earth's lower mantle. Science 310, 297–299.

Tackley, P.J., 1996. Effects of strongly variable viscosity on three-dimensional compressible convection in planetary mantles. J. Geophys. Res. B 101, 3311–3332.

Tackley, P.J., Stevenson, D.J., 1993. A mechanism for spontaneous self-perpetuating volcanism on the terrestrial planets. In: Stone, D.B., Runcorn, S.K. (Eds.), Flow and Creep in the Solar System: Observations, Modeling, and Theory. Kluwer Academic Publ.

Tarduno, J.A., Cottrell, R.D., Watkeys, M.K., Bauch, D., 2007. Geomagnetic field strength 3.2 billion years ago recorded by single silicate crystals. Nature 446, 657–660. doi:10.1038/nature05667.

Thorne, M.S., Garnero, E.J., 2004. Inferences on ultralow-velocity zone structure from a global analysis of SPdKS waves. J. Geophys. Res. 109, B08301.

Williams, Q., Garnero, E.J., 1996. Seismic evidence for partial melt at the base of the Earth's mantle. Science 273, 1528–1530.